ASEAN Engineering Journal

Full Paper

SHRIMP SHELL-BASED ACTIVATED CARBON: EFFECTIVE AND ROBUST ADSORBENT FOR REMOVAL OF IRON ION

Trung Quoc Tran[a,b], Thanh Kien Huynh[b,c], Tung Thanh Duong[b,c], Minh-Anh Huynh Le[b,c], Thanh Khoa Phung[b,c,*]

[a]Faculty of Chemical Engineering, Ho Chi Minh City University of Technology (HCMUT), 268 Ly Thuong Kiet Street, Ho Chi Minh City, Vietnam
[b]Viet Nam National University Ho Chi Minh City, Vietnam
[c]Department of Chemical Engineering, School of Chemical and Environmental Engineering, International University, VNU-HCM, Ho Chi Minh City, Vietnam

Article history
Received
03 September 2025
Received in revised form
15 December 2025
Accepted
04 February 2026
Published online
31 August 2026

*Corresponding author
ptkhoa@hcmiu.edu.vn

Graphical abstract

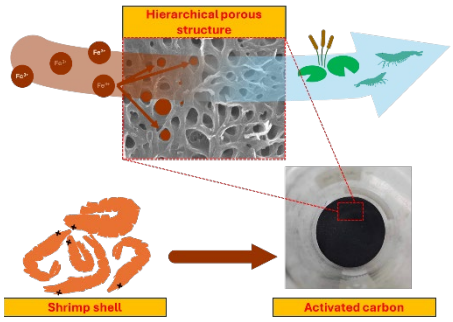

Abstract

Heavy metal pollution has posed a significant threat to environmental and human health. In this work, activated carbon synthesized from shrimp shells through KOH activation was employed as an adsorbent for Fe^{3+} ion removal from aqueous solutions. The material was characterized using X-ray diffraction, scanning electron microscopy, and N_2 adsorption/desorption analysis. Batch adsorption experiments were conducted to assess the adsorption capacity of the activated carbon, while the effects of initial ion concentration, contact time, pH, and adsorbent dosage were analyzed using Response Surface Methodology. The results showed that the adsorption process followed pseudo-second-order kinetics, indicating a chemisorption mechanism. While the Langmuir isotherm effectively described the adsorption behavior. The results also showed that a maximum removal efficiency of 72.31% was achieved at the optimal conditions (19.131 mg/L initial concentration, pH 6, and 130.394 minutes). The findings revealed that shrimp shell–derived activated carbon displayed strong adsorption efficiency for Fe^{3+} ions. This study contributes to the development of eco-friendly and cost-effective materials for heavy metal removal and underscores the significance of utilizing waste materials for value-added purposes in the field of environmental science and engineering.

Keywords: Activated carbon; Fe^{3+} ions; Freundlich isotherm; heavy metal; Langmuir isotherm

1.0 INTRODUCTION

Water is an essential resource for sustaining life and supporting sustainable development on Earth. It is critical not only for human survival but also for key economic sectors such as agriculture, industry, energy, and transportation [1]. However, growing challenges such as rapid population growth, industrialization, and inefficient groundwater and soil management have increasingly led to water scarcity and pollution [2, 3]. Water pollution has become a pressing global concern, and Vietnam is no exception [4]. Pollutants including heavy metals and organic impurities greatly affect ecological systems and public health. Among heavy metals, iron is an essential trace element for living organisms, excessive concentrations—above 0.3 mg/L—can lead to adverse health effects, including nausea and dizziness [5]. Furthermore, iron levels exceeding 1.8 mg/L can impart a noticeable metallic taste to drinking water [6]. High iron content also causes water turbidity, stains fabrics, and contributes to the clogging of pipelines.

To remove heavy metals from wastewater, several physical and chemical treatment technologies have been developed including filtration, acid precipitation, coagulation and flotation, sedimentation, and biochemical degradation [7,

8]. Other techniques were also applied such as solvent extraction, membrane filtration, air flotation [9], and phytoremediation [10] for the removal of heavy metals. Specific methods like sorption and aeration are also commonly integrated into wastewater treatment systems [11, 12]. Among these, adsorption has emerged as a widely used approach due to its effectiveness and simplicity. A range of adsorbent materials—such as activated carbon, silica, and others—are employed to remove metal contaminants from various types of wastewater [13].

Among various adsorbent materials including porous zeolites [14], silica gel [15], metal-organic frameworks (MOFs) [16], activated alumina [5], carbon nanotubes [17], and activated carbon [18-20], activated carbon stands out due to its high carbon content and versatile performance. Its most notable feature is its highly porous structure, which leads to an exceptionally large surface area. Activated carbon (AC) can be produced from Coconut Shell [21], *Bambusa vulgaris* (AC surface area ~ 1042 m^2/g) [18], corncob-based (1600 m^2/g) [22]; activated carbon aerogels (2600 m^2/g) [23]; and sugarcane bagasse-derived (3555 m^2/g) [24]. This extensive surface area provides abundant active sites for adsorption, enabling efficient removal of target contaminants from gas or liquid phases. Therefore, there are many studies focusing on using activated carbon for the heavy metal adsorption [25-28].

In this work, activated carbon was prepared from shrimp shell waste and utilized for the adsorption of iron (Fe) ions. Shrimp shells were selected as the raw material due to their high availability in Vietnam—one of the world's leading shrimp exporters, with an export turnover reaching USD 3.9 billion in 2024 (VASEP) [29]. Additionally, Yu et al. reported that shrimp shell rich in calcium could act as native pore templates, and avoid the disadvantages of activated carbon derived from agricultural resources such as additional treatments in the production of activated carbon [30]. Indeed, the activated carbon from shrimp shell in this study showed a promising maximum Fe ion adsorption capacity of 66.67 (mg/g), indicating a potential material for adsorption. Therefore, converting this abundant waste into high-value materials like activated carbon represents a sustainable and economically viable waste management strategy.

2.0 METHODOLOGY

2.1. Materials

The shrimp shell utilized in this study was obtained from Ca Mau Seafood Co., Ltd., located in Ca Mau, Vietnam. To ensure the removal of impurities, the shell was thoroughly cleaned with deionized water and subsequently subjected to sun-drying. Next, the shell underwent coarse crushing and sieving.

Metal ion Fe^{3+} solution was prepared by using iron (III) nitrate nonahydrate (Fisher Scientific, 98%). All experimental solutions were appropriately diluted using deionized water. Potassium hydroxide (86%), sodium hydroxide (97%), and hydrochloric acid (37%) were supplied by Fisher Scientific Co., Ltd. (USA). NaOH (Xilong Scientific, analytical grade) and HCl (Xilong Scientific, analytical grade) were employed as chemical agents to adjust the pH levels, with the aid of a pH meter (METTLER TOLEDO).

2.2. Preparation Of Activated Carbon

The activated carbon (AC) was synthesized by using an in-house fabricated tubular furnace (Figure S1) for carbonization and a KOH activation, with a few changes to the previously described procedure [31]. Firstly, a porcelain boat carrying 10 g of shrimp shell powder (particle size of 125-212μm) was placed in the furnace. The carbonization process was executed under the nitrogen flow (50 cc/min) with a temperature program of an increase from room temperature to 600 °C with a ramp of 10 °C/min, and hold for 2 h [32]. The biochar obtained (~ 70% biomass yield) was let to cool down. Next, biochar was thoroughly mixed with KOH powder a mass ratio of 2:1 using a spatula and activated at 750 °C for 1.5 h after increasing temperature from room temperature to 750 °C with a ramp of 10 °C/min in nitrogen atmosphere. The resulting material was subsequently washed with 1 M HCl solution and deionized water using a vacuum filtration system until reaching neutral pH, followed by drying at 80 °C overnight. The yield of activated carbon is ca. 15% of initial shrimp shell. Biochar (without activation) sample was denoted as AC-0, while the AC-KOH sample represented activated carbon.

2.3. Characterization

To examine the crystallinity of the samples, the crystalline structure was characterized by XRD using a Shimadzu 6100 diffractometer (Shimadzu Corporation, Kyoto, Japan) under operating conditions of a voltage of 40 kV and a current of 30 mA, using CuK_α radiation (wavelength λ = 1.5406 nm). Scans were recorded from 10° to 60° (2θ) at a step interval of 0.02° and a speed of 0.05°/s. The Brunauer-Emmett-Teller (BET) surface area was determined by a nitrogen adsorption/desorption isotherm method at – 200 °C with 30 adsorption points and 16 desorption points using a Nova4000e (Quantachrome) instrument. A JEOL JSM-IT200 microscope (JOEL Ltd., Tokyo, Japan) was employed to characterize the surface morphology of the material after gold coating.

2.4. Adsorption Study

Adsorption experiments were conducted by adding 0.025 g of the AC-KOH sample into 25 mL of metal ion solution containing in a 50 mL conical flask and stirring at 200 rpm using a magnetic stirrer at room temperature (25 °C). The effects of pH (2–6), initial ion concentration (C_o = 5–70 mg/L), and contact time (t = 10–180 min) were investigated. The Fe^{3+} concentration was set at 6.9, 13.9, 27.7, 41.6, 55.4 and 69.3 mg/L. While the adsorption time set at 10, 20, 30, 40, 60, 90, 120, and 180 minutes, with different pH of 2, 3, 4, 5, and 6. After adsorption, the AC-KOH sample was separated from the solution via gravity filtration, and the residual Fe^{3+} concentration was determined using a UV-Vis spectrophotometer (Jasco V-730) at the maximum absorption wavelength of 300 nm. All experiments were duplicate.

The Fe^{3+} removal (%) in solution was evaluated according to Eq. (1).

$$Fe^{3+}\ \text{removal}\ (\%) = \frac{C_0 - C}{C_0} \times 100\% \quad (1)$$

where C_0 and C is the before and after adsorption concentration of Fe^{3+} (mg/L)

The Fe^{3+} uptake is assessed by the Eq. (2):

$$q_e = \frac{(C_0 - C_e) \times V}{m} \quad (2)$$

where q_e represents the adsorption capacity of AC-KOH (mg/g); C_o and C_e denote the initial and equilibrium concentrations of Fe^{3+} in solution, respectively; V is the solution volume (L); and m is the adsorbent mass (g).

Response surface methodology (RSM) was applied using a three-factor Box–Behnken design (BBD) to model the relationship among variables influencing Fe^{3+} removal from aqueous solution. Three independent parameters were investigated including pH, initial Fe^{3+} concentration and adsorption time. The experiment design is illustrated in Table S1. The statistical program Design Expert Software was used to create a total of 17 trials.

3.0 RESULTS AND DISCUSSION

3.1 XRD pattern

XRD patterns present the impact of carbonization and KOH activation processes on the crystallinity of activated carbons (Figure 1). The AC-0 (biochar) produced from carbonization process of shrimp shell possessed high crystallinity primarily due to the presence of CaO and $CaCO_3$. The diffraction peaks at 23.0°, 29.4°, 36.0°, 39.4°, 43.1°, 47.0°, 48.5°, 57.4° attributed to the planes of (012), (104), (110), (113), (202), (018), (116), and (122), respectively, indicating the presence of $CaCO_3$ (JCPDS card no. 96-901-6707) [33]. While the presence of CaO was demonstrated with the peaks at 32.2° , 37.3°, and 53.8° corresponding to (111), (200) and (220) planes, respectively (JCPDS card no. 01-1160) [34]. The AC-KOH material activated with KOH after the carbonization process exhibited amorphous graphitized structure.

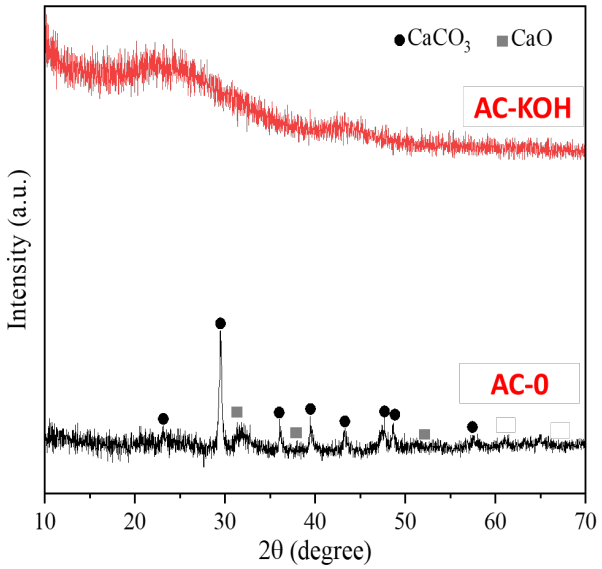

Figure 1 XRD patterns of the AC-0 and AC-KOH materials

3.2 Textural Properties

Figure 2 presents the isotherm and distribution of pore diameter of the AC-KOH sample. The isotherm of the AC-KOH sample exhibited a type-IV characteristic (Figure 2a), suggesting the coexistence of micropores and mesopores [35]. Additionally, the H4 hysteresis loop of the AC-KOH sample showed the pore properties of this sample with narrow slit-like and ink-bottle sharped pores. Looking at the pore distribution, average pore diameter is 15.774 Å demonstrating the presence of mesopores (Figure 2b). Moreover, the volume of micropores occupies ca. 45% of total volume of pores (Table S2). This observation suggests that the majority of the pore structures in the AC-KOH material is micropore.

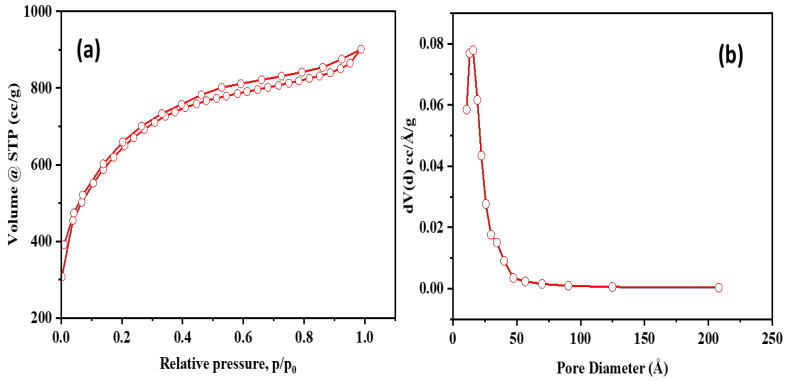

Figure 2 (a) BET isotherm and (b) pore diameter distribution of the AC-KOH material

3.3 SEM Images

The morphology of the AC-0 (biochar) and AC-KOH materials are illustrated in SEM images (Figure 3). The AC-0 material exhibited a negligible hollow structure (Figure 3a) indicating low surface area [36]. Following the activation, the non-porous structure of biochar underwent a transformation into porous activated carbon (AC-KOH). SEM images revealed the porous structure of the AC-KOH material (Figure 3b). This morphological characteristic was expected to be efficient in adsorption processes. In fact, during the activation process of shrimp shells using KOH, KOH reacted with carbon of biochar via the reaction $6KOH + 2C \rightarrow 2K + 2H_2 + 2K_2CO_3$ resulting in the formation of holes (pores) of activated carbon. Carbon of biochar also decomposed through following reactions of carbon with K_2CO_3, CO_2, K_2O as reported in previous study [32]. These reactions led to enhance the pore of activated carbon resulting the formation of porous material.

Moreover, the EDX analysis showed the rich in carbon of the activated carbon material (Table S3) confirming the successful activated carbon synthesis.

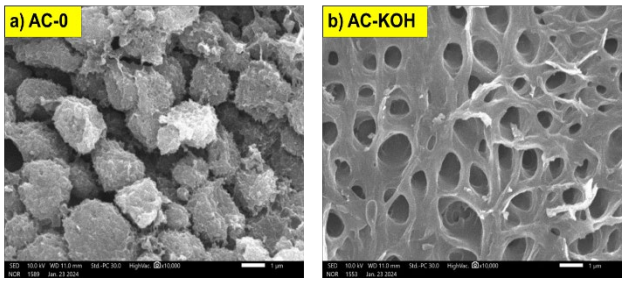

Figure 3 SEM images of (a) AC-0 and (b) AC-KOH samples

3.4 Adsorption Study

3.4.1 Effect Of Adsorption Time

The equilibrium time of adsorption was governed by the interplay between contact time and adsorption capacity. The Fe^{3+} uptake onto the AC-KOH sample dramatically increased within the first 40 minutes, then reached equilibrium after that (Figure 4a). The rapid adsorption of Fe^{3+} cation on the AC-KOH sample was owing to the fast diffusion of Fe^{3+} cation on the surface of the AC-KOH sample. Once all available sites were occupied, equilibrium was established after 40 minutes.

3.4.2 Effect Of PH On Fe^{3+} Adsorption Capacity

To investigate the influence of pH, experiments were conducted at a fixed initial Fe^{3+} ion concentration of 27.73 mg/L and an adsorption time of 40 minutes, with pH values varied from 2 to 6. Figure 4b showed that the higher the pH is, the better the performance of the AC-KOH sample in Fe^{3+} adsorption is. These findings can be explained that the adsorbent surface carries a positive charge at lower pH making cation adsorption unfavorable. This occurs because hydrogen ions strongly compete with metal ions for adsorbing on the active sites, thereby restricting adsorption. However, a higher in Fe^{3+} removal efficiency at pH of 3 was noted, indicating the emergence of another chemical phenomena. Partial hydrolysis of Fe^{3+} in a basic medium can produce hydroxyl complexes, including $Fe(OH)^{2+}$ and $Fe(OH)_4^-$ [37]. Therefore, the involvement of Fe-hydroxyl species in adsorption and/or precipitation on the adsorbent surface can occur [38].

3.4.3 Kinetic Study

To study the adsorption kinetics, the adsorption was carried out at pH 2, 0.025 g AC-KOH at room temperature. The kinetic behavior of Fe^{3+} adsorption onto AC-KOH sample was analyzed using pseudo-first-order (Eq. 3), pseudo-second-order (Eq. 4), and Elovich (Eq. 5) models [39].

Pseudo-1st order equation:

$$\ln(q_e - q_t) = \ln(q_e) - k_1 t \quad (3)$$

Pseudo-2nd order equation:

$$\frac{t}{q_t} = \frac{1}{k_2 q_e^2} + \frac{1}{q_e} t \quad (4)$$

The Elovich equation:

$$q_t = \frac{1}{\beta}\ln(\alpha\beta) + \frac{1}{\beta}\ln t \quad (5)$$

In these models, k_1 (1/min) and k_2 (g/mg·min) are the rate constants, α is the initial adsorption rate (mg/g·min), and β corresponds to the desorption constant. The adsorption capacities at equilibrium and at time t are denoted as q_e and q_t (mg/g), respectively. The experimental results were scattered to determine which kinetics model fitted the best (Figure 5). A higher correlation coefficient was obtained for the pseudo-second-order model compared to the pseudo-first order and Elovich models, confirming its better agreement with the experimental results (Figure 5). Moreover, the theoretical q_e value showed close agreement with the experimental q_e obtained from the pseudo-second-order model (Table 1), suggesting that chemisorption is the primary mechanism governing the rate-determining step [40].

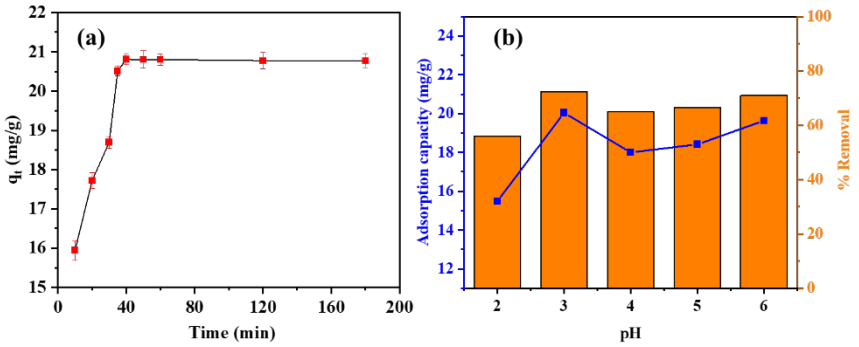

Figure 4 Effect of (a) adsorption time and (b) pH on Fe^{3+} removal on the AC-KOH material at pH 3, initial Fe^{3+} concentration of 27.73 mg/L, and 25 °C.

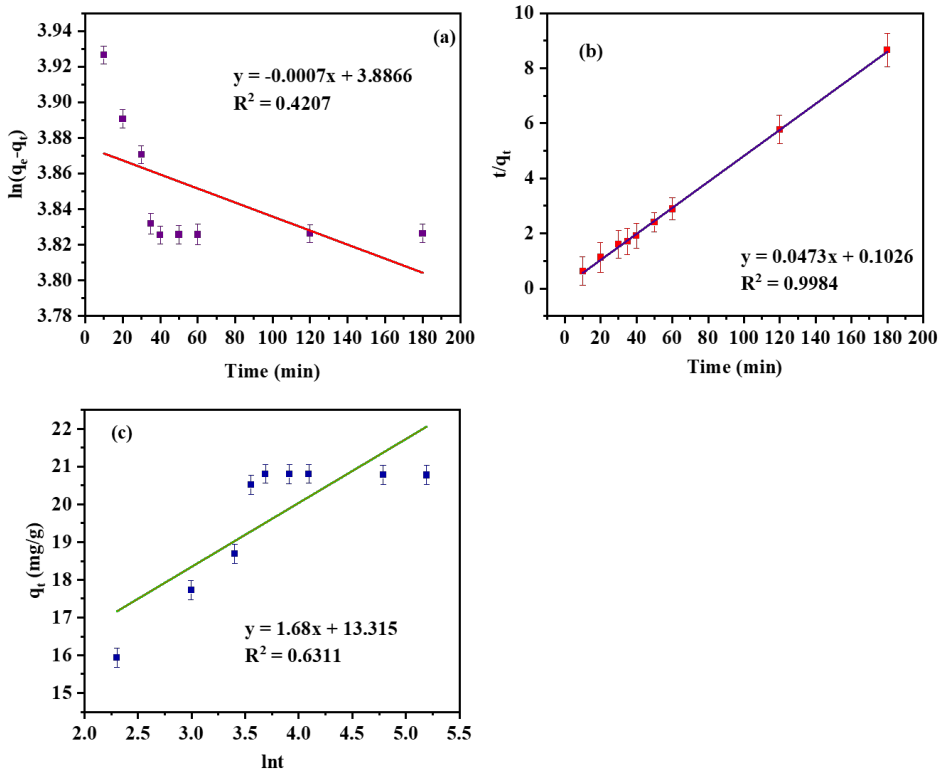

Figure 5 a) Pseudo-1st order, b) Pseudo-2nd order and c) Elovich adsorption kinetic model for Fe^{3+} removal on the AC-KOH material at pH 3, initial Fe^{3+} concentration of 27.73 mg/L, and 25 °C.

Table 1 Kinetic constants for Fe^{3+}adsorption

Pseudo – 1st constant			Pseudo – 2nd constant			Elovich constant			q_e exp (mg/g)
q_e (mg/g)	k_1	R^2	q_e (mg/g)	k_2	R^2	β	α	R^2	
48.74	0.0007	0.4207	21.4592	0.0167	0.9984	0.595	4645.08	0.6311	20.8092

3.4.4 Adsorption Isotherms

The behavior of the adsorbate at the equilibrium point is represented by adsorption isotherms [41]. To study the adsorption isotherms, the adsorption time was fixed for 40 minutes based on kinetic results, where Fe^{3+} uptake rapidly increased during the first 40 minutes and then plateaued, indicating saturation of active sites. Typical adsorption isotherm

models, namely Langmuir and Freundlich, were applied to describe the adsorption behavior in this study. The Langmuir and Freundlich isotherm models were selected because they represent two fundamental adsorption mechanisms: monolayer adsorption on homogeneous surfaces (Langmuir) and multilayer adsorption on heterogeneous surfaces (Freundlich).

The Langmuir isotherm, which describes monolayer adsorption on the adsorbent surface, represented using Eq. (6) in nonlinear form or Eq. (7) in linear form [42]:

$$q_e = \frac{q_{max} b C_e}{1 + b C_e} \quad (6)$$

or

$$\frac{C_e}{q_e} = \frac{1}{q_{max} b} + \frac{C_e}{q_{max}} \quad (7)$$

For multilayer adsorption, the Freundlich isotherm was used [43]. Either Eq. (8) (nonlinear form) or Eq. (9) (linear form) corresponds to the Freundlich isotherm [44]:

$$q_e = k C_e^{1/n} \quad (8)$$

Or

$$\ln q_e = \ln K_f + \frac{1}{n} \ln C_e \quad (9)$$

In these equations, q_e represents the adsorption capacity at equilibrium (mg/g), q_{max} the maximum adsorption capacity (mg/g), and C_e the equilibrium concentration of Fe^{3+} (mg/L). The Langmuir constant b (L/mg) describes adsorption affinity, whereas the Freundlich constants K_f and n indicate the properties of the adsorbent and the adsorption intensity, respectively. Adsorption is favorable when n falls within the range of 1–10.

Figure S2 illustrates the linear relation between C_e/q_e versus C_e in Langmuir equation, and the linear plot between $\ln C_e$ and $\ln q_e$ in Freundlich equation. The values of q_{max}, a, b, and K_f were summarized in Table 2. Both isotherm models adequately described the adsorption process ($R^2 > 0.96$), but the equilibrium adsorption of Fe^{3+} exhibited better agreement with the Langmuir model. The highest estimated adsorption capacity (q_{max}) was 66.67 mg/g.

Table 2 The constants for the adsorption of Fe^{3+} in the Langmuir and Freundlich models.

Langmuir constant				Freundlich constant		
q_{max} (mg/g)	b (L/mg)	R_L	R^2	n	K_f	R^2
66.67	0.0655	0.36	0.9837	1.84	7.34	0.9617

3.4.5 Optimal adsorption study

Optimization of the adsorption process was performed using Response Surface Methodology (RSM) with a Box–Behnken design based on a quadratic model comprising 12 runs and 5 center points. The comparison of anticipated and experimental values for the removal of Fe^{3+} is shown in Table S4. From the experimental results, an empirical relationship was derived between the response (Y) and the coded independent variables (x_1, x_2, x_3). The Box–Behnken design was then applied to generate a quadratic equation for predicting the optimal conditions.

$$Y = 56.30 + 16.23x_1 - 7.81x_2 + 6.24x_3 - 5.14x_1x_2 + 0.6436x_1x_3 - 1.81x_2x_3 - 5.31x_1^2 - 12.12x_2^2 - 9.49x_3^2 \quad (10)$$

The maximum removal capacity was obtained of 72.31% at required conditions (pH = 6; C_0 = 19.13 mg/L; t = 130.39 minutes) (Table 3). An analysis of variance (ANOVA) was performed to statistically assess the significance of both the main and interaction effects of factors on the adsorption process within the regression model. The ANOVA analysis of the quadratic equation demonstrates that the model and the correlation between the response and key variables generated a value of 175.72 (Table S5). This finding suggests that the likelihood of such a substantial "Model F-value" occurring solely due to random variability is only 0.01%. This indicates that the majority of the response's variation can be illustrated by the regression equation. Therefore, the statistical significance of the model is confirmed. Furthermore, the statistical significance of the model is reinforced by the extremely small probability value ($p < 0.0001$). Within the scope of this study, it is determined that the factors x_1, x_2, x_3, x^2_1, x_1x_2, x_1x_3, and x_2x_3 exhibit significant effects. In contrast, model terms with p-values exceeding 0.1 in Table S5 are considered statistically insignificant. The "Lack-of-Fit F-value" is used to assess the model's capability to represent data points beyond the regression fit. The relatively low F-value of 3.60 suggests a lack of statistical significance. While Lack-of-Fit F-values (12.39%) may be attributed to random fluctuations which serve as additional validation of the quadratic model. The results also reveal that variables x_1 and x show a positive correlation with Fe^{3+} removal. Moreover, the coefficient of determination (R^2) is employed to assess the results. The "Predicted R^2" value of 0.9467 aligns reasonably well with the "Adjusted R^2" value of 0.9899. The "Adequacy Precision" serves as an indicator of the signal-to-noise ratio, of which values surpassing 4 are deemed desirable. In this case, the ratio of 38.4388 for the AC-KOH sample represents an adequate signal, thereby suggesting the effective applicability of this model in exploring the design space [45].

Table 3. Maximum Fe^{3+}removal (%) under optimum conditions

Adsorbent	x_1: pH	x_2: C_0 (mg/L)	x_3: t (min)	Fe^{3+} removal (%)	Desirability
AC-KOH	6	19.131	130.394	72.31	0.875

The data was systematically evaluated to assess the relationship between the experimental and predicted values of responses for the AC-KOH sample as shown in Figure 6. The plot revealed that the data points were well-scattered and closely aligned with a linear trend, exhibiting a high R^2 value of 0.955 for the AC-KOH sample. The obtained R^2 values indicated a strong agreement between the experimental and predicted responses of the adsorbents, confirming the suitability of the selected quadratic model for estimating response variables from the experimental data [46].

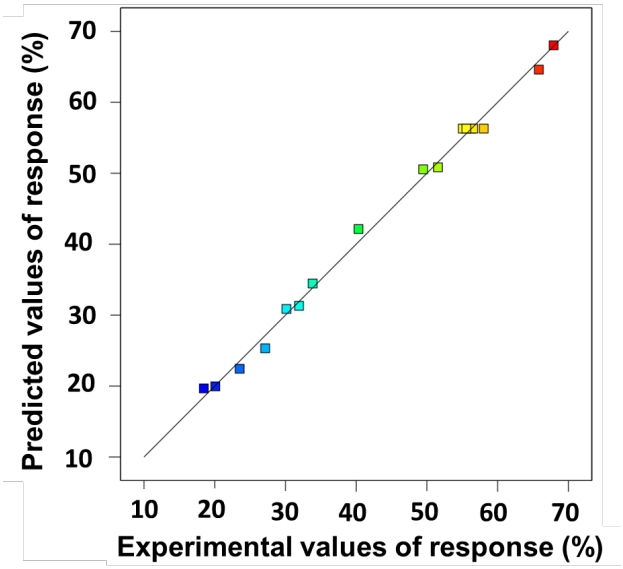

Figure 6 Correlation between the response's actual and expected values for the AC-KOH sample

Moreover, the standard error plot showed a minimum value of 0.437 near the centroid (Figure S3), indicating that the model reliably guides the experimental design space for Fe^{3+} adsorption on the AC-KOH sample. In addition, it demonstrates the model's reliability in accurately estimating the response and provides valuable insights for the design process.

Furthermore, a three-dimensional (3D) surface plot was employed as an envisioning tool for the impact of interactive variables on Fe^{3+} adsorption on the AC-KOH sample (Figure 7). Figure 7a illustrates the impact of pH (2, 4, and 6) and initial Fe^{3+} ion concentration (5, 37.5, and 70 mg/L) on the adsorption capacity, in which, the adsorption time was maintained at a constant value of 95 minutes. Figure 7a shows that the highest Fe^{3+} removal efficiency occurred at pH 6 with an initial Fe^{3+} concentration of 5 mg/L. Additionally, an important parameter in adsorption studies is the pH as it determines the environment to facilitate the adsorption process. Figure 7a also demonstrates that increasing the pH leads to a higher Fe^{3+} uptake, indicating a positive correlation. This can be explained by the elevated concentration of hydronium ions (H_3O^+) in the solution at lower pH levels. Consequently, H_3O^+ ions compete with Fe^{3+} ions for the active binding sites on the adsorbent surface. The intensified competition for binding sites reduces the adsorption efficiency, resulting in a lower percentage of Fe^{3+} removal [47]. A higher pH leads to less competition from hydronium ions and less electrostatic repulsion between cations and the surface sites, which promotes improved metal adsorption [48].

A 3D surface plot analysis possibly assesses how the solution pH and adsorption time affect the adsorption process. The adsorption behavior was evaluated at pH 2–6 with a fixed Fe^{3+} concentration of 37.5 mg/L (Figure 7b). Fe^{3+} removal improved as pH increased from 2 to 6, accompanied by longer adsorption times (10–180 min). The maximum removal efficiency for Fe^{3+} was achieved at pH 6 in 180-minute intervals. The Fe^{3+} removal efficiency was also assessed across initial concentrations of 5–70 mg/L and adsorption time (Figure 7c). The pH remained constant at 4, serving as the central level. The result demonstrates that the adsorption capacity of the AC-KOH sample from 5 to 70 mg/L, and the adsorption time slightly increased from 10 to 180 minutes.

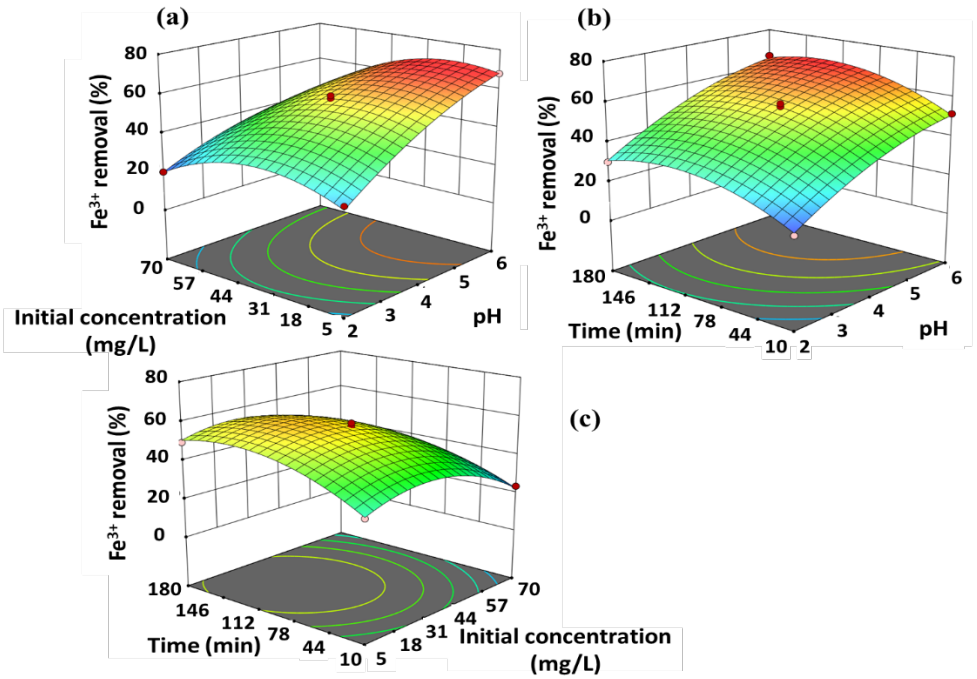

Figure 7 Effects of (a) pH and initial metal concentration, (b) pH and adsorption time, and (c) initial metal concentration and adsorption time on adsorption of Fe^{3+} by the AC-KOH material by response surface plot in three dimensions

Table 4 Comparison of the iron removal by adsorption method

Entry	material source	Adsorbent	Maximum Fe ion adsorption capacity (mg/g)	The highest Fe removal efficiency (%)	Ref.
1	Banana peel	Activated carbon	10.02 (Fe^{2+})	-	[49]
2	sugarcane bagasse	Activated carbon	55.55 (Fe^{2+})	-	[50]
3	coconut shell	Activated carbon	0.17	99	[51]
4	*Bombax ceiba* fruit shell	Activated carbon	37.16	99.10	[52]
5	corn cob	Activated carbon	334.9	89.3	[53]
6	luffa sponge	Activated carbon	317.1	79.9	[53]
7	crab shell	Activated carbon	1.08	-	[54]
8	-	Chitosan flakes	> 80	-	[55]
9	Shrimp shell	Activated carbon	66.67	72.31	This study

Table 4 summarized the comparison of the iron removal by adsorption method using activated carbon and other adsorbents. The activated carbon derived from shrimp shell exhibited a promising maximum Fe ion adsorption capacity (66.67 mg/g) in comparison to the literature (Table 4). The adsorption capacity of AC in this study is lower than that of AC from corn cob and luffa sponge [53], and comparable with chitosan fakes [55], but higher than that of AC from other biomass (Table 4, entry 1-4, 7). For the Fe removal efficiency, activated carbon of this study is close to the literature suggesting that this AC can be applied to remove iron ions as well as heavy metals.

The successful synthesis of activated carbon from waste shrimp shells enhances the use of waste, leading to the potential application of converting waste into valuable products and reducing environmental impact. However, the yield of activated carbon is still lower than expected. Also, the recycling of activated carbon for iron adsorption has to be tested to confirm the stability of material. Therefore, the preparation method needs to be improved to increase activated carbon yield, resulting in a lower-cost AC product, as well as the requirement of a stability test.

4.0 CONCLUSION

In this study, hierarchical porous activated carbon was synthesized from shrimp shells via 2 main steps including carbonization and activation with KOH applying for the iron removal. The results showed that activated carbon synthesized possesses porous structure with high surface area (~2291 m^2/g). Adsorption efficiency was strongly influenced by time, pH, initial Fe^{3+} concentration, and adsorbent dosage. The Langmuir isotherm model is the adsorption behavior of Fe^{3+} onto AC, and the adsorption process followed pseudo-second-order kinetics. The activated carbon exhibited excellent adsorption performance for Fe^{3+} ion. The highest removal efficiency (72.31%) was obtained at an initial concentration of 19.13 mg/L, pH 6, and 130.39 minutes. The maximum adsorption capacity for Fe^{3+} ion was 66.67 mg/g, and this result is comparable to activated carbon from other resources making it a potential application in the industry. Additionally, this activated carbon may enhance the adsorption capacity and yield by modifying the preparation method. In short, the results demonstrate that activated carbon from waste shrimp shells exhibits promising, eco-friendly, and cost-effective adsorption capacity and efficiency, making it a viable option for environmental remediation applications.

Acknowledgement

This research is funded by International University, VNU-HCM under grant number T2023-01-SEE.

Conflicts of Interest

The author(s) declare(s) that there is no conflict of interest regarding the publication of this paper

References

[1] Kılıç, Z., 2020, "The importance of water and conscious use of water," *International Journal of Hydrology*, 4(5): 239-241.

[2] Wu, P., and M. Tan, 2012, "Challenges for sustainable urbanization: a case study of water shortage and water environment changes in Shandong, China," *Procedia Environmental Sciences*, 13: 919-927.

[3] Yap, C. N., and T. Hadibarata, 2022, "Remediation of contaminated soil with crude oil by composting," *Journal of Civil Engineering*, 13(1): 49-58.

[4] Chu, A. D., M. C. Pham, and M. K. Nguyen, 2010, "Characteristic of urban wastewater in Hanoi City–nutritive value and potential risk in using for agriculture," *VNU Journal of Science: Earth and Environmental Sciences*, 26(1): 42-47

[5] Rajurkar, N. S., A. N. Gokarn, and K. Dimya, 2011, "Adsorption of chromium (III), nickel (II), and copper (II) from aqueous solution by activated alumina," *Clean–Soil, Air, Water*, 39(8): 767-773.

[6] Adam, C., J. Baudin, and J. Garnier-Laplace, 2001, "Kinetics of 110mAg, 60Co, 137Cs and 54Mn bioaccumulation from water and depuration by the crustacean Daphnia magna," *Water, Air, and Soil Pollution*, 125: 171-188.

[7] Tahir, M. S., M. Sagir, and M. B. Tahir, 2023, Advances in Water and Wastewater Treatment Technology, Springer Nature.

[8] Vertinsky, A., "Problems of the current state of physico-chemical methods of wastewater treatment," Proc. AIP Conference Proceedings, AIP Publishing LLC, p. 020003.

[9] Tansel, B., 2008, "New technologies for water and wastewater treatment: A survey of recent patents," *Recent patents on chemical engineering*, 1(1): 17-26.

[10] Balamoorthy, D., P. Velusamy, B. Rath, P. T R, and J. Kabeto, 2022, "Removal of heavey metals from astewater by using phytoremediation technology," *Journal of Civil Engineering, Science and Technology*, 13(1): 23-32.

[11] Littman, H., J. L. Plawsky, and J. D. Paccione, 2014, "Waste Water Treatment Apparatus and Methods."

[12] Mao, G., Y. Han, X. Liu, J. Crittenden, N. Huang, and U. M. Ahmad, 2022, "Technology status and trends of industrial wastewater treatment: A patent analysis," *Chemosphere*, 288: 132483.

[13] Sharma, Y. C., V. Srivastava, V. Singh, S. Kaul, and C. Weng, 2009, "Nano-adsorbents for the removal of metallic pollutants from water and wastewater," *Environmental technology*, 30(6): 583-609.

[14] Shavandi, M., Z. Haddadian, M. H. S. Ismail, N. Abdullah, and Z. Abidin, 2012, "Removal of Fe (III), Mn (II) and Zn (II) from palm oil

mill effluent (POME) by natural zeolite," *Journal of the Taiwan institute of chemical engineers*, 43(5): 750-759.

[15] Zhu, Y., Y. Niu, H. Li, B. Ren, R. Qu, H. Chen, and Y. Zhang, 2018, "Removal of Cd (II) and Fe (III) from DMSO by silica gel supported PAMAM dendrimers: Equilibrium, thermodynamics, kinetics and mechanism," *Ecotoxicology and Environmental Safety*, 162: 253-260.

[16] Peng, Y., H. Huang, Y. Zhang, C. Kang, S. Chen, L. Song, D. Liu, and C. Zhong, 2018, "A versatile MOF-based trap for heavy metal ion capture and dispersion," *Nature communications*, 9(1): 187.

[17] Gao, Y., L. Pan, H. Li, Y. Zhang, Z. Zhang, Y. Chen, and Z. Sun, 2009, "Electrosorption behavior of cations with carbon nanotubes and carbon nanofibres composite film electrodes," *Thin Solid Films*, 517(5): 1616-1619.

[18] Mistar, E., S. Ahmad, A. Muslim, T. Alfatah, and M. Supardan, "Preparation and characterization of a high surface area of activated carbon from Bambusa vulgaris—Effect of NaOH activation and pyrolysis temperature," Proc. *IOP Conference Series: Materials Science and Engineering,* 012051. IOP Publishing

[19] Kavand, M., P. Eslami, and L. Razeh, 2020, "The adsorption of cadmium and lead ions from the synthesis wastewater with the activated carbon: Optimization of the single and binary systems," *Journal of Water Process Engineering*, 34: 101151.

[20] Mohamad Said, K. A., M. A. Mohamed Amin, I. Yakub, M. R. Rahman, A. B. Hong Kueh, S. Hamdan, and M. M. Rahman, 2023, "Methylene Blue Adsorption Mechanism onto Palm Kernel Shell-derived Activated Carbon: From Particle Diffusion to Site Adsorption," *BioResources*, 18(3): 5120-5132

[21] Yakub, I., K. A. M. Said, M. A. M. Amin, A. B. H. Kueh, and M. Amran, 2024, "Aqueous-phase Reforming of Glycerol using Cu-Ni Bimetal Catalyst Supported over Coconut Shell Activated Carbon," *Journal of Advanced Research in Fluid Mechanics and Thermal Sciences*, 115(1): 193-205.

[22] Tsai, W., C. Chang, S. Wang, C. Chang, S. Chien, and H. Sun, 2001, "Preparation of activated carbons from corn cob catalyzed by potassium salts and subsequent gasification with CO2," *Bioresource technology*, 78(2): 203-208.

[23] Hanzawa, Y., K. Kaneko, R. Pekala, and M. Dresselhaus, 1996, "Activated carbon aerogels," *Langmuir*, 12(26): 6167-6169.

[24] Dwiyaniti, M., A. E. Barruna, R. M. Naufal, I. Subiyanto, R. Setiabudy, and C. Hudaya, "Extremely high surface area of activated carbon originated from sugarcane bagasse," *Proceeding IOP Conference Series: Materials Science and Engineering*, 012018. IOP Publishing.

[25] Pereira, L., V. Castillo, M. Calero, G. Blázquez, R. R. Solís, and M. Ángeles Martín-Lara, 2024, "Conversion of char from pyrolysis of plastic wastes into alternative activated carbons for heavy metal removal," *Environmental Research*, 250: 118558.

[26] Mkilima, T., Y. Zharkenov, A. Abduova, N. Sarypbekova, N. Kudaibergenov, K. Sakanov, G. Zhukenova, Z. Omarov, P. Sultanbekova, and G. Kenzhaliyeva, 2024, "Utilization of banana peel-derived activated carbon for the removal of heavy metals from industrial wastewater," *Case Studies in Chemical and Environmental Engineering*, 10: 100791.

[27] Saikia, S., V. Anagha, M. Khwairakpam, and A. S. Kalamdhad, 2024, "Assessment of activated carbon derived from municipal solid waste char as a precursor for mitigation of heavy metals," *Biomass and Bioenergy*, 190: 107385.

[28] Tounsadi, H., M. Khnifira, A. Khalidi, M. Abdennouri, and N. Barka, 2025, "Effective removal of heavy metals from aqueous solutions using activated biomass: Analytical interpretation via molecular dynamic simulation, mathematical and statistical approaches," *Journal of Molecular Structure*, 1319: 139371.

[29] VASEP, 2025, "Infographic: Vietnam shrimp exports in 2024," https://vasep.com.vn/san-pham-xuat-khau/infographic/infographic-xuat-khau-tom-viet-nam-nam-2024-32619.html. Retrieved on September 2, 2025

[30] Yu, J., L. Tang, Y. Pang, G. Zeng, H. Feng, J. Zou, J. Wang, C. Feng, X. Zhu, X. Ouyang, and J. Tan, 2020, "Hierarchical porous biochar from shrimp shell for persulfate activation: A two-electron transfer path and key impact factors," *Applied Catalysis B: Environmental*, 260: 118160.

[31] Guo, J., Y. Song, X. Ji, L. Ji, L. Cai, Y. Wang, H. Zhang, and W. Song, 2019, "Preparation and characterization of nanoporous activated carbon derived from prawn shell and its application for removal of heavy metal ions," *Materials*, 12(2): 241.

[32] Pham, X.-T., V. A. Tran, L.-T. T. Tran, T. N. P. Nguyen, T. H. Le, H. Hoang, T.-H. Nguyen, K. B. Vu, and T. K. Phung, 2022, "Hierarchical Porous Activated Carbon-Supported Ruthenium Catalysts for Catalytic Cleavage of Lignin Model Compounds," *Energies*, 15(22): 8611.

[33] Diningsih, C., and L. Rohmawati, 2022, "Synthesis of calcium carbonate (CaCO3) from eggshell by calcination method," *Indonesian Physical Review*, 5(3): 208-215.

[34] Zhang, Y., and F. Liu, 2015, "End to end assembly of CaO and ZnO nanosheets to propeller-shaped architectures by orientation attachment approaches," *Journal of Crystal Growth*, 420: 94-100.

[35] Xiao, Y., C. Long, M.-T. Zheng, H.-W. Dong, B.-F. Lei, H.-R. Zhang, and Y.-L. Liu, 2014, "High-capacity porous carbons prepared by KOH activation of activated carbon for supercapacitors," *Chinese Chemical Letters*, 25(6): 865-868.

[36] Muniandy, L., F. Adam, A. R. Mohamed, and E.-P. Ng, 2014, "The synthesis and characterization of high purity mixed microporous/mesoporous activated carbon from rice husk using chemical activation with NaOH and KOH," *Microporous and Mesoporous Materials*, 197: 316-323.

[37] Aryal, M., and M. Liakopoulou-Kyriakides, 2013, "Binding mechanism and biosorption characteristics of Fe (III) by Pseudomonas sp. cells," *Journal of Water sustainability*, 3(3): 117-131.

[38] Dideriksen, K., J. Baker, and S. Stipp, 2006, "Iron isotopes in natural carbonate minerals determined by MC-ICP-MS with a 58Fe–54Fe double spike," *Geochimica et Cosmochimica Acta*, 70(1): 118-132.

[39] Rudzinski, W., and W. Plazinski, 2006, "Kinetics of solute adsorption at solid/solution interfaces: a theoretical development of the empirical pseudo-first and pseudo-second order kinetic rate equations, based on applying the statistical rate theory of interfacial transport," *The Journal of Physical Chemistry B*, 110(33): 6514-16525.

[40] Sahoo, T. R., and B. Prelot, 2020, "Adsorption processes for the removal of contaminants from wastewater: the perspective role of nanomaterials and nanotechnology," Nanomaterials for the detection and removal of wastewater pollutants, Elsevier, 161-222.

[41] Lesoin, L., C. Crampon, O. Boutin, And E. Badens, 2011, "CO2/water/surfactant ternary systems and liposome formation using supercritical CO2: A review," Colloids and Surfaces A: Physicochemical and Engineering Aspects, 377(1–3): 1-14.

[42] Liu, Y., 2006, "Some consideration on the Langmuir isotherm equation," *Colloids and Surfaces A: Physicochemical and Engineering Aspects*, 274(1-3): 34-36.

[43] Okoniewska, E., J. Lach, M. Kacprzak, and E. Neczaj, 2007, "The removal of manganese, iron and ammonium nitrogen on impregnated activated carbon," *Desalination*, 206(1-3): 251-258.

[44] Ng, C., J. N. Losso, W. E. Marshall, and R. M. Rao, 2002, "Freundlich adsorption isotherms of agricultural by-product-based powdered activated carbons in a geosmin–water system," *Bioresource technology*, 85(2): 131-135.

[45] Kiran, B., and K. Thanasekaran, 2011, "Copper biosorption on Lyngbya putealis: application of response surface methodology (RSM)," *International Biodeterioration & Biodegradation*, 65(6): 840-845.

[46] Yetilmezsoy, K., S. Demirel, and R. J. Vanderbei, 2009, "Response surface modeling of Pb (II) removal from aqueous solution by Pistacia vera L.: Box–Behnken experimental design," *Journal of hazardous materials*, 171(1-3): 551-562.

[47] Vasu, A. E., 2008, "Adsorption of Ni (II), Cu (II) and Fe (III) from aqueous solutions using activated carbon," *Journal of Chemistry*, 5: 1-9.

[48] Esfandiar, N., B. Nasernejad, and T. Ebadi, 2014, "Removal of Mn (II) from groundwater by sugarcane bagasse and activated carbon (a comparative study): Application of response surface methodology (RSM)," *Journal of industrial and engineering chemistry*, 20(5): 3726-3736.

[49] Yanti, I., P. P. Sationo, W. F. Winata, M. Anugrahwati, A. K. Anas, and Y. A. Swasono, 2023, "Effectiveness of activated carbon magnetic composite from banana peel (Musa acuminata) for recovering iron metal ions," *Case Studies in Chemical and Environmental Engineering*, 8: 100378.

[50] Braz, G. S., J. d. C. L. Carvalho, J. G. de Andrade, A. T. D. Junior, R. P. de Lima, E. N. Lima, O. E. Ferreira, M. A. de Oliveira, A. C. d. S. Bezerra, and A. R. T. Machado, 2025, "Adsorption of ferrous ions onto phosphoric acid-activated biochar," *Desalination and Water Treatment*, 321: 100958.

[51] Thinojah, T., and B. Ketheesan, 2022, "Iron removal from groundwater using granular activated carbon filters by oxidation coupled with the adsorption process," *Journal of Water and Climate Change*, 13(5): 1985-1994.
[52] Brishti, R. S., R. Kundu, M. A. Habib, and M. H. Ara, 2023, "Adsorption of iron(III) from aqueous solution onto activated carbon of a natural source: Bombax ceiba fruit shell," *Results in Chemistry*, 5: 100727.
[53] El-Bendary, N., H. k. El-Etriby, and H. Mahanna, 2021, "High-performance removal of iron from aqueous solution using modified activated carbon prepared from corn cobs and luffa sponge," *Desalination and Water Treatment*, 213: 348-357.
[54] Porpino, K. K. P., M. d. C. S. Barreto, K. B. Cambuim, J. R. d. Carvalho Filho, I. A. S. Toscano, and M. d. A. Lima, 2011, "Fe (II) adsorption on Ucides cordatus crab shells," *Química Nova*, 34: 928-932.
[55] Costea, I. F., A.-M. Ceoromila, A. Tabacaru, and G. Carac, 2024, "Investigation of Chitosan Flakes in the Adsorption of Fe (III) Ions from Acidic Solution," *Revista de Chimie*, 75(2): 1-10.

Appendix

Table S1 Variable types and experimental levels in the Box-Behnken statistical model

Independent factors	Symbol	Coded variable level		
		Low	Center	High
		-1	0	1
pH	x_1	2	4	6
Initial Fe^{3+} concentration (mg/L)	x_2	5	37.5	70
Adsorption time (min)	x_3	10	95	180

The number of experiments was determined by the Eq. (1):

$$N = k^2 + k + cp \quad (1)$$

where cp is the number of times the center point reoccurs, and k is the number of variations.
The values of the process variables that were coded were determined using Eq. (2):

$$x_i = \frac{X_i - X_0}{\Delta X_i} \qquad i = 1,2,3,\ldots,k \quad (2)$$

where x_i is the independent variable's uncoded value; X_i is the dimensionless coded value; X_o is the value of X_i at the center point; and ΔX_i is the step change value. The following general Eq. (3) represents the applied quadratic response model:

$$Y = \beta_0 + \beta_1 x_1 + \beta_2 x_2 + \beta_3 x_3 + \beta_{11} x_1^2 + \beta_{22} x_2^2 + \beta_{33} x_3^2 + \beta_{12} x_1 x_2 + \beta_{13} x_1 x_3 + \beta_{23} x_2 x_3 + \varepsilon \quad (3)$$

where Y is the dependent variable, β_0 is constant, β_1, β_2, β_3 are first order (linear) coefficient, β_{11}, β_{22}, β_{33} are the quadratic (squared) coefficient, β_{12}, β_{13}, $\beta 2_3$ are the interaction coefficient; x_i is coded independent variables, specifically pH (x_1), initial Fe^{3+} concentration (x_2) and adsorption time (x_3); ε is the random error or the variance between anticipated and measured values [1].

Table S2 The BET surface area, pore volume and average diameter of the AC-KOH sample

Sample	Surface area S (m^2/g)	S_{micro}/S	Total volume of pores V_p (cc/g)	V_{micro}/V_p	Average diameter of pores D_p (Å)
AC-KOH	2291.3	0.325	1.448	0.453	15.774

S_{micro}: Surface area of micropores (m^2/g)
V_{micro}: volume of micropores (cc/g)

Table S3 EDS analysis of activated carbon derived from shrimp shell

Samples	% Mass				
	C	O	Si	S	Cl
AC-0	93.61	4.76	0.37	0.91	0.35
AC-KOH	92.74	6.07	0.54	0.52	0.13

Table S4 Actual and predicted response values in Box-Behnken experiments

Standard order	Run	Factor 1 x_1: pH	Factor 2 x_2: C_0 (mg/g)	Factor 3 x_3: Adsorption time (min)	Fe^{3+} removal (%)	
					AC-KOH	
					Actual value	Predicted value
1	15	2	5	95	27.14	25.32
2	3	6	5	95	67.92	68.04
3	5	2	70	95	20.08	19.96
4	2	6	70	95	40.33	42.14
5	10	2	37.5	10	18.45	19.67
6	7	6	37.5	180	51.57	50.84
7	16	2	37.5	180	30.14	30.87
8	12	6	37.5	10	65.82	64.61
9	14	4	5	10	33.85	34.46
10	4	4	70	180	23.52	22.44
11	1	4	5	180	49.47	50.56
12	13	4	70	10	31.92	31.32
13	6	4	37.5	95	56.25	56.30
14	17	4	37.5	95	56.54	56.30
15	11	4	37.5	95	55.08	56.30
16	9	4	37.5	95	58.04	56.30
17	8	4	37.5	95	55.58	56.30

Table S5 The response surface quadratic model (Y) underwent analysis of variance (ANOVA)

Source	SS[a]	df [b]	MSS[c] MSS = SS/df, $MSS_E = SS_E/df_E$	F value F_{cal}= MSS/MSS_E	P value (Prob>F)
Model	4258.36	9	473.15	175.72	< 0.0001[d]
x_1	2106.83	1	2106.83	782.45	< 0.0001[d]
x_2	488.54	1	488.54	181.44	< 0.0001[d]
x_3	311.95	1	311.95	115.85	< 0.0001[d]
x_1^2	105.48	1	105.48	39.17	0.0004[d]
x_2^2	1.66	1	1.66	0.6154	0.4585
x_3^2	13.03	1	13.03	4.84	0.0637
x_1x_2	118.88	1	118.88	44.15	0.0003[d]
x_1x_3	618.30	1	618.30	229.63	< 0.0001[d]
x_2x_3	379.02	1	379.02	140.76	< 0.0001[d]
Residual	18.85	7	2.69	-	-
Lack of fit	13.75	3	4.58	3.60	0.1239
Pure error	5.09	4	1.27	-	-
Cor total	4277.21	16	-	-	-

[a] Sum of squares

[b] Degree of freedom

[c] Mean sum of squares

[d] Significant at p values < 0.05

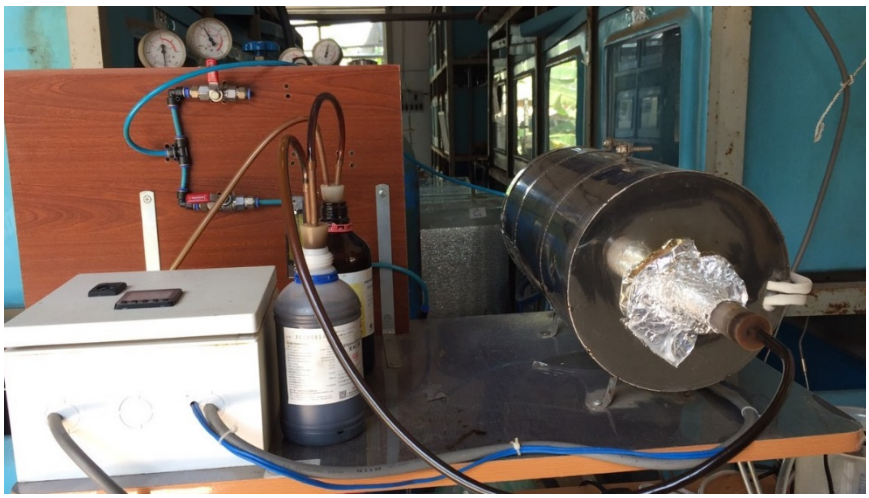

Figure S1 The photograph of an in-house fabricated tubular furnace

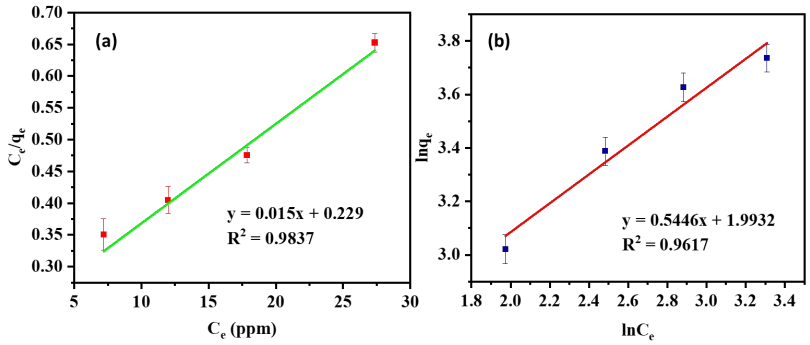

Figure S2 (a) Langmuir and (b) Freundlich adsorption isotherm for Fe^{3+} removal on the AC-KOH material at condition (pH: 3, C_e: (27.73, 41.58, 55.44, 69.30) mg/L, temperature: 25 $\pm$ 1°C)

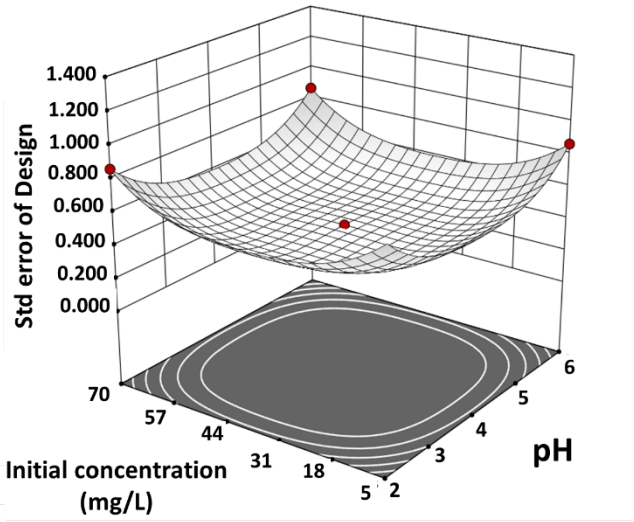

Figure S3 Standard error plot in three-dimensions for the adsorption of Fe^{3+} by the AC-KOH sample